Posteriori estimation of low altitude propagation loss from radar sea clutter data

Peter Gerstoft
Marine Physical Laboratory
Scripps Institution of Oceanography
La Jolla, CA 92093-0238

L. Ted Rogers
Atmospheric Propagation Branch
SPAWAR Systems Center
San Diego, CA 92152

William S. Hodgkiss
Marine Physical Laboratory
Scripps Institution of Oceanography
La Jolla, CA 92093-0238

Abstract— **This paper describes the estimation of propagation loss and it statistical properties based on observations of radar sea clutter data. This problem is solved by first finding an ensemble (about 10^5 models) of relevant refractivity model parameters and then using all these models to map into the propagation loss domain. In this mapping each refractivity model is weighted according to its data likelihood function.**

I. INTRODUCTION

Historically, the vertical profile of atmospheric refractivity of a "standard atmosphere" has been used as a basis for radar performance predictions. Since the mid-1980's it has become common practice to improve this profile with surface observations of air temperature, sea temperature, wind speed and relative humidity, in conjunction with an atmospheric surface-layer model to estimate the refractivity profile within the marine atmospheric surface layer [1]. The refractivity profile above the surface layer is not characterized by the surface layer models and is usually characterized by weather-balloons or rocket-sondes [2]. But whereas the surface layer measurements can be made continuously, weather-balloons or rocket soundings are expensive in both use of expendables and manpower. An alternative means for estimating refractivity for the purpose of radar performance assessment is to use radar clutter (e.g., Fig. 1) as described by the authors in [3], [4].

A general weakness of all methods employed in estimating radar performance has been the lack of a means for quantifying the impact of uncertainty in the estimates of refractivity that the performance estimates are based on. This might be a particular concern when using radar clutter for the characterization. Consider Fig. 2: A pattern of radar clutter over tens of kilometers on a given azimuth is observed. Unknown to us, however, are how random processes in individual range bins, and colored processes in range (i.e., horizontal gradients in wind speed, hence the sea clutter radar cross section) have affected the pattern. In the context of our forward modeling, though, this makes the observation somewhat uncertain. Many different realizations of refractivity—possibly from disjoint regions in the environmental parameter space—map into the region of uncertainty surrounding our observation.

The principle of the inversion is indicated in Fig. 2. From the observed radar clutter data or the data-space **d**, a prediction of propagation loss, the information usage domain **u**, is searched. The vector **d** represents the obseved radar data at N range
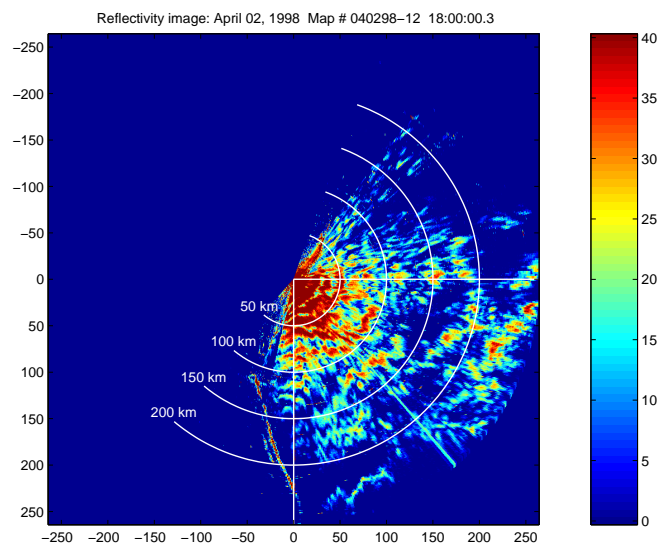

Fig. 1.   Clutter map from SPANDAR corresponding to Wallops Run 12.

bins and the vector **u** represents a vector of propagation loss at certain height and range bins. This involves a number of steps as outlined below:

(1) Determine a model for the refractive environment (Appendix of [3]) and select an appropriate propagation model (e.g., TPEM [5]). These two form the mapping $\mathbf{d}(\mathbf{m})$ from the parameter space **m** to data space **d**. The vector **m** represents the unknown environmental parameters.

(2) Determine the mapping $\mathbf{u}(\mathbf{m})$ from the parameter space to information usage space. Except for a change in geometry (receiver height), this is similar to $\mathbf{d}(\mathbf{m})$.

(3) Find acceptable models **m** from the data. As indicated in Fig. 2, a region around the data can map into several acceptable solutions in the model domain.

(5) Map the acceptable models into the data usage domain.

(6) The posteriori results, both in parameter **m** and data utility **u** domains should be interpreted probabilistically.

As indicated in Fig. 2, this mapping is non-unique. There are many solutions that give about the same goodness-of-fit. The maximum likelihood (ML) is the best fit of all. In particular we can associate cost (or risk) from errors in the solution—a reasonable assumption in this problem—and the uncertainty of the solution is non-uniform in the data usage space. Knowing
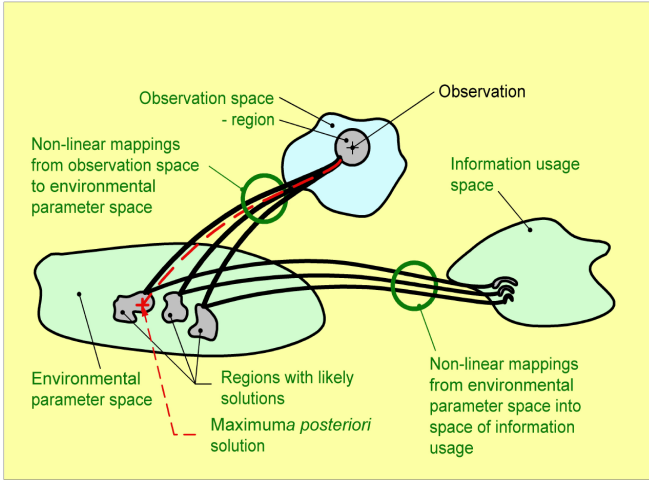
Fig. 2. Mappings between observed radar clutter data $\mathbf{d}$, environmental parameters $\mathbf{m}$ and the propagation loss usage domain $\mathbf{u(m)}$.

the posteriori distribution or part thereof is preferable to having a single point estimate such as the ML solution.

A. Replica generation

The replica clutter return $\mathbf{d(m)}$ is modeled as follows:
1. An environmental model maps the environmental parameters $\mathbf{m}$ into modified refractivity as a function of range r and height z.
2. A combined radar and propagation model maps modified refractivity into radar observations $\mathbf{d}_0(\mathbf{m})$.

For solving of the inverse problem, a large number (about 90.000) realizations of the replica have to be generated.

II. INVERSE PROBLEM FRAMEWORK

In the Bayesian paradigm, the solution to determining parameters of interest $\mathbf{m}$ given an observation $\mathbf{d}$ is characterized by the posteriori probability $p_p(\mathbf{m}\,|\,\mathbf{d})$. A clear discussion on on inverse theory from a probabilistic point of view is given by [6]. Additional details of Monte Carlo sampling of posteriori probabilities is given by [7], [8], [9], [10], [11].

Following Mosegaard and Tarantola [10], represent the inverse problem as conjuncture of information. The posteriori distribution $p_p(\mathbf{m,d})$ is given by

$$p_p(\mathbf{m,d}) = p_e(\mathbf{m,d})p_a(\mathbf{m,d}) \ , \qquad (1)$$

where $p_a(\mathbf{m,d})$ is the prior probability and $p_e(\mathbf{m,d})$ is the probability obtained from the experiment. We note that this is quite similar to the Bayesian approach.

The joint prior theoretical probability is constructed as follows: First the marginal prior probability $p(\mathbf{m})$ is used to generate samples of $\mathbf{m}$ and then via the forward model $u(\mathbf{m})$ the joint prior probability distribution $p(\mathbf{m,d(m)})$. It should be noted that this is not just a simple mapping as $\mathbf{d(m)}$ contains additional noise and shifting of the clutter in range has been added to the clutter return via Markov chains. Note, that the construction does not involve any observed data and thus can be precomputed.

The experimental probability is based on the likelihood formulation in Sect. III. The objective function $\phi(\mathbf{d,d(m)})$ is a squared error (Sect. III).

From the joint posteriori distribution $p_p(\mathbf{m,d})$, we obtain the posteriori distribution $p_p(\mathbf{m})$ of the environmental parameters

$$p_p(\mathbf{m}) = \int_{\mathcal{D}} p_p(\mathbf{m,d}) \, d\mathbf{d} \ . \qquad (2)$$

This distribution contains all relevant information and from this distribution all relevant features of the environment can be found as the most common value of $\mathbf{m}$ in $p_p(\mathbf{m})$ is the maximum *a posteriori* (MAP) estimator.

We are not interested in the environment itself but rather better estimates of the parameters in the information usage domain $\mathbf{u(m)}$. Based on the posteriori distribution $p_p(\mathbf{m})$, the distribution of $p_p(\mathbf{u(m)})$ is obtained and from this distribution all relevant statistics of the usage space can be obtained.

A. Probability of utility information $\mathbf{u}$

Both the experimental data $\mathbf{d}$ and the utility data $\mathbf{u}$ are related to $\mathbf{m}$ via forward models $F(\mathbf{m})$ and $G(\mathbf{m})$ corresponding to $\mathbf{d(m)}$ and $\mathbf{u(m)}$. Thus formally we have $\mathbf{u} = G(F^{-1}(\mathbf{d}))$. However, this direct mapping is ill posed and is instead interpreted based on conjuncture of information whereby we can also include prior information. Similar to Eq. 1 the posteriori probability is obtained

$$p_p(\mathbf{u,m,d}) = p_e(\mathbf{u,m,d})p_a(\mathbf{u,m,d}) \ . \qquad (3)$$

Often the prior probabilities are independent and the above equation can be simplified

$$p_p(\mathbf{u,m,d}) = p_e(\mathbf{u,m,d})p_a(\mathbf{u})p_a(\mathbf{m})p_a(\mathbf{d}) \ . \qquad (4)$$

We obtain the marginal *posteriori* distribution $p_p(\mathbf{u})$

$$p_p(\mathbf{u}) = \int_{\mathcal{D}} \int_{\mathcal{M}} p_p(\mathbf{u,m,d}) \, d\mathbf{m}d\mathbf{d} \ . \qquad (5)$$

Often the posteriori distribution of $p_p(\mathbf{m})$ is first obtained and from this the probability distribution of the propagation loss is obtained

$$p_p[u(r,z)] = \int u(r,z,\mathbf{m})p_p(\mathbf{m}) \, d\mathbf{m} \qquad (6)$$

From this distribution all relevant statistical features of the propagation loss can be obtained, as for example the mean and variation of the propagation loss

$$\mathsf{E}\,[u\,(r,z)] = \int u(r,z)p_p[u(r,z)] \, du \qquad (7)$$

$$\mathsf{Var}\,[u\,(r,z)] = \int \left(u\,(r,z) - \mathsf{E}\,[u(r,z)]\right)^2 p_p[u(r,z)] \, du \qquad (8)$$

III. LIKELIHOOD AND OBJECTIVE FUNCTION

The likelihood and the objective function are derived assuming a simple linear model

$$\mathbf{d} = S\mathbf{d}(\mathbf{m}) + \mathbf{e} \ . \tag{9}$$

the scalar S represents unknown radar strength and calibration constants. $\mathbf{d}$ and $\mathbf{d}(\mathbf{m})$ represents measuered and modelled data organized into a vector of N data points, corresponding to each range bin. $\mathbf{m}$) repensent the M environmental parameter to be determined. Assuming the errors $\mathbf{e}$ to be Gaussian distributed with mean $S\mathbf{d}(\mathbf{m})$ and standard deviation $\mathbf{C}$. The errors represent all features that are not modeled in the data as noise, theoretical errors, and modeling errors. This is a reasonable model for high signal-to-error ratio, but for low signal-to-error ratio this is not a good assumption [8]. The likelihood function is

$$L(\mathbf{m}) = (\pi|\mathbf{C}|)^{-N} \exp\left(-[\mathbf{d} - S\mathbf{d}(\mathbf{m})]^{\dagger}\mathbf{C}^{-1}[\mathbf{d} - S\mathbf{d}(\mathbf{m})]\right) \ . \tag{10}$$

where N is the number of data points. As usual, we assume $\mathbf{C} = \nu\mathbf{I}$ The source S can be estimated in closed form by requiring $\partial \log L/\partial S = 0$, whereby

$$S^{\mathrm{ML}} = \frac{\mathbf{d}^{\dagger}\mathbf{d}(\mathbf{m})}{\|\mathbf{d}(\mathbf{m}\|^2} \tag{11}$$

It is seen that S depends on $\mathbf{m}$ but not on ν. The likelihood function is then

$$L(\mathbf{m}) = (\pi\nu)^{-N} \exp\left(-\phi(\mathbf{m})/\nu\right) \tag{12}$$

where

$$\phi(\mathbf{m}) = \mathbf{d}^2 - \left(\frac{\mathbf{d}^{\dagger}\mathbf{d}(\mathbf{m})}{\|\mathbf{d}(\mathbf{m}\|}\right)^2 \ , \tag{13}$$

is the objective function. The likelihood estimate of the noise ν^{ML} can be estimated in closed form by solving $\partial \log L/\partial \nu = 0$,

$$\nu^{\mathrm{ML}} = \phi(\mathbf{m})/N \ . \tag{14}$$

Reinserting this into the likelihood function gives

$$L(\mathbf{m}) = \left(\frac{N}{\pi\mathrm{e}\phi(\mathbf{m})}\right)^N \ . \tag{15}$$

The ML solution $\mathbf{m}^{\mathrm{ML}}$ is obtained by maximizing the objective function over all $\mathbf{m}$. Finally, an overall estimate for the error power ν is obtained from (14) at the environmental ML solution: $\nu^{\mathrm{ML}}(\mathbf{m}^{\mathrm{ML}})$ and can be re-inserted into the likelihood function. For simplicity, we consider the error as known and only keep the free argument $\mathbf{m}$ of the objective function ϕ. This approach leads to [8]

$$\mathcal{L}(\mathbf{m}) = \left[\frac{N}{\pi\phi(\mathbf{m}^{\mathrm{ML}})}\right]^N \exp\left[-N\frac{\phi(\mathbf{m})}{\phi(\mathbf{m}^{\mathrm{ML}})}\right] \ . \tag{16}$$

However, posteriori densities also can be based on (15). The expressions (15) and (16) differ in their error estimates: In (15), the error power is estimated for each geoacoustic model vector $\mathbf{m}$. In (16) the global ML estimate of the error power

Model parameter	Lower bound	Upper bound
Base height, z_{b} (m)	0	400
M-deficit, M_{d} (M-units)	0	250
Thickness, z_{thick} (m)	0	150
Slope (M-units/m)	-1	0.13
Evaporation duct height (m)	0	50

TABLE I

INVERSION MODEL WITH PARAMETER SEARCH BOUNDS. THESE PARAMETER BOUNDS WERE USED BOTH AT THE INITIAL RANGE ($r = 0$) AND AT THE FINAL RANGE ($r = 100\mathrm{KM}$). FOR ALL RANGES EACH PARAMETER WAS LINEARLY INTERPOLATED.
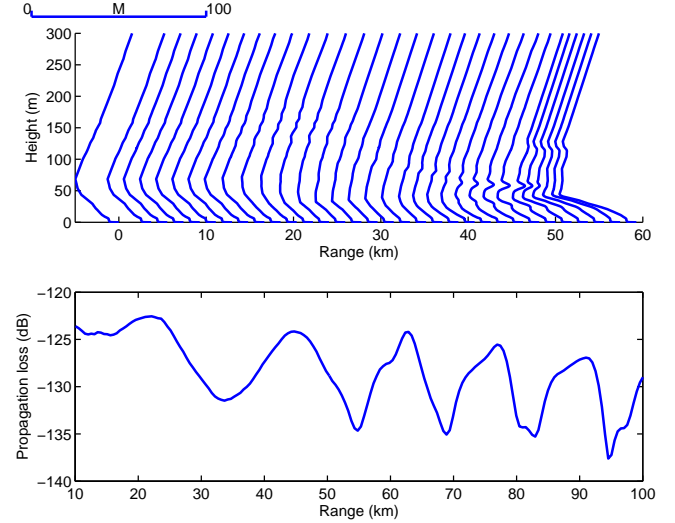

Fig. 3. The refractivity profile (a) used to generate the data, and (b) the propagation loss data.

(which was found from optimization) is posteriori estimated and then is (as a prior) applied to all model vectors $\mathbf{m}$ [8].

The above derivation assumes that the error in each sample is uncorrelated with the next sample. In practice these are strongly correlated and therefore the number of samples N in the above equations must be replaced with the effective number of samples, N_{eff}.

IV. EXAMPLE

The data are generated based on the helicopter measured range-dependent refractivity profiles (Run 7) for the Wallops 98 experiment [3]. These profiles were interpolated using the LARRI program [12]. A range interval from 10-100 km is used. A simple trilinear model is used for the refractivity profile as outlined in the Appendix of [3]. We then search for refractivity parameters at 0 and 100 km range with unknown parameters as given in Table I. To obtain refractivity profiles at other ranges the parameters are interpolated linearly. The first 3 parameters were given a uniform distribution but the slope was given a non-uniform distribution as indicated in Fig 4 (left bottom). This is because a negative slope is only likely for shallow ducts.

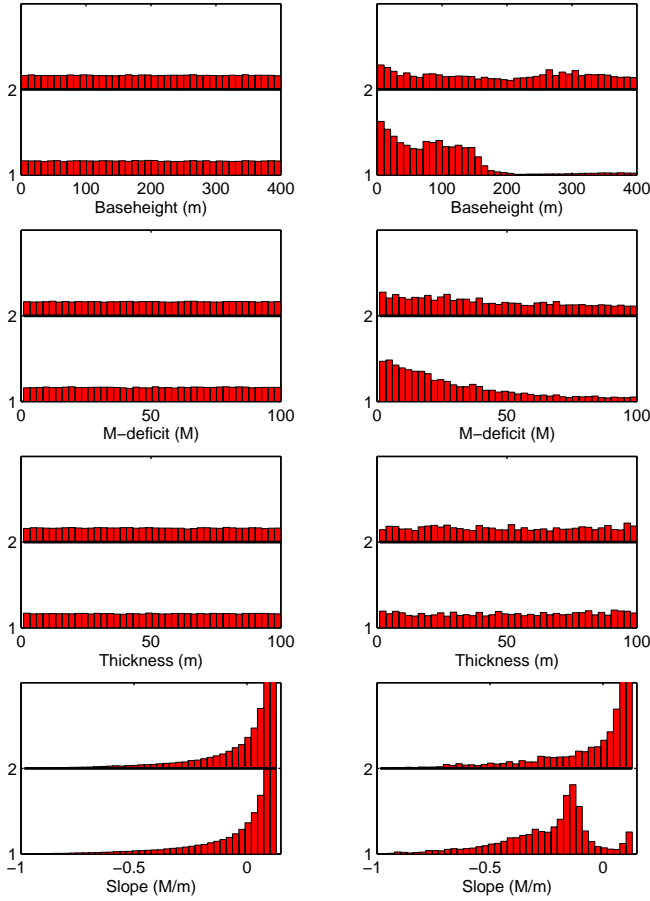Using this environmental model, 90,000 replicas are precomputed. To compute the prior distribution of the envi-

Fig. 4.   Prior (left) and posteriori (right) distributions of the parameter estimates.
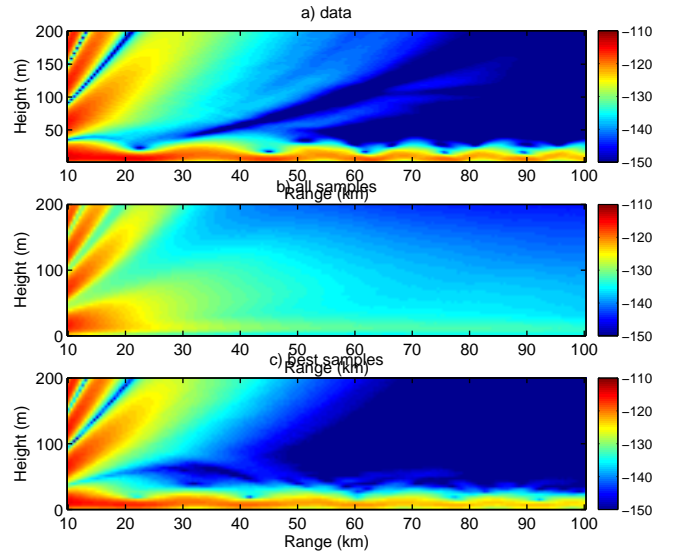

Fig. 5.   The propagation-loss field based on (a) the true environment (from Fig. 3a), based on (b) prior information, and (c) posteriori information (bottom).
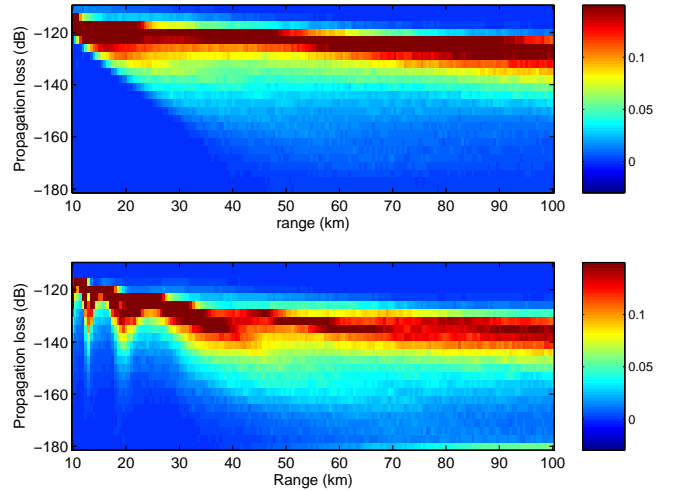

Fig. 6.   Prior probability distribution for propagation loss versus range at 10 m (top) and 100 m (bottom) height.

ronmental parameters all samples are weighted evenly (left column Fig. 4). The smoothness of these indicate that the prior is well sampled. To compute the posteriori distribution (right column Fig. 4) Eqs. (3) and (16) are used. We note that the overall behavior seems reasonable. A more robust convergence criterium [9] will indicate that the distributions are not yet completely converged.

The important issue is to be able to estimate statistics of posteriori propagation loss. Figs. 5–9 illustrate this estimation. We compute the priori propagation loss based on an even weighting of the propagation loss from each generated refractivity model. The posteriori probability distribution of the propagation loss is based on weighting the propagation loss from each refractivity model with the posteriori probability, Eq. (6).

The average   prior propagation loss and the posteriori propagation loss are shown in Fig. 5b and c. It is seen that the posteriori propagation loss identifies a ducting environment as observed in the data, Fig. 5a, but the prior does not.

The probability distribution of the field then is computed. Both prior field (Fig. 6) and the posterior field (Fig. 7) are calculated at 10 and 100 m height as a function of range. Figure 8 shows the probability distribution at 50 km range and 10 m height. This corresponds to a simple cut though the

contour plots in Figs. 6 and 7.

Based on the distribution of propagation loss, the mean and standard deviation are computed as a function of range (10–100 km) in the duct (12-m height) or above the duct (102-m height), see Fig. 9. Clearly, the posteriori distribution is much more compact for the lower height than for the higher height — a behavior that is expected given that the input data is effectively a (somewhat) contaminated direct measure of the propagation loss at the surface.

V. SUMMARY

An algorithm for estimating statistical properties of propagation loss based on refractivity from radar clutter has been described using a likelihood formulation. The likelihood function is developed assuming the error in the data to be Gaussian.
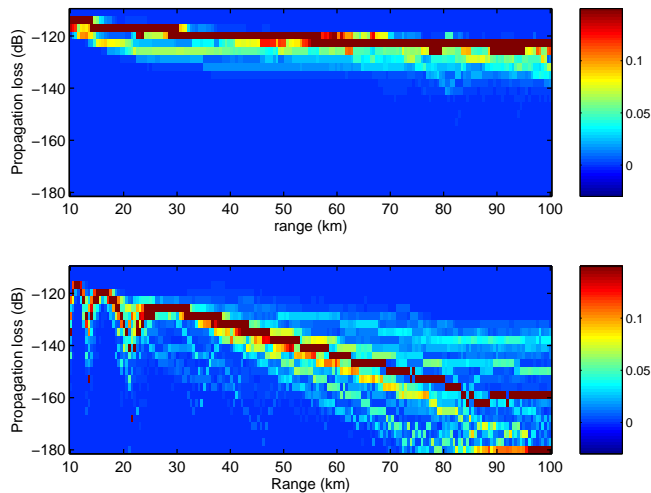
Fig. 7. Posteriori probability distribution for propagation loss versus range at 10 m (top) and 100 m (bottom) height.
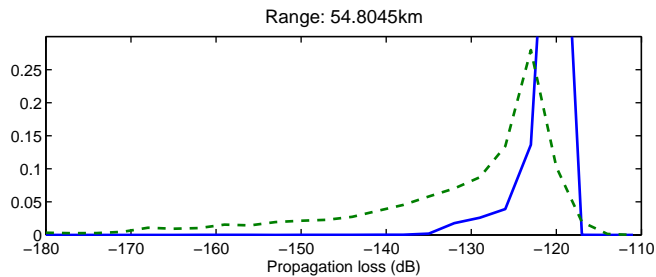

Fig. 8. Posteriori (solid) and prior (dashed) probability at 50 km range and 10 m height.
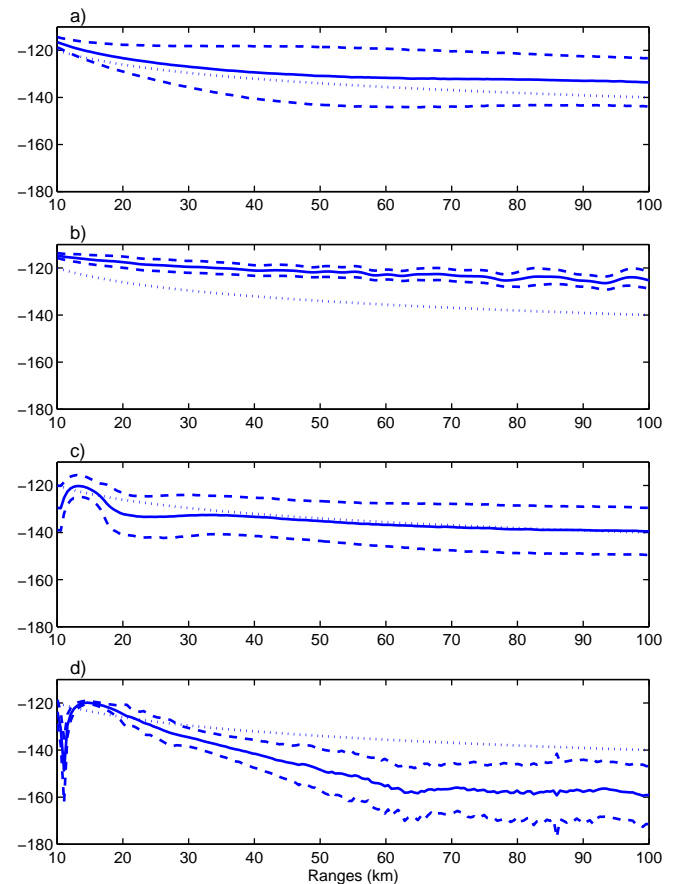

Fig. 9. The average field (solid) and plus/minus one standard deviation (dashed) based on all prior samples (a and c) and just the best posteriori samples (b and d) at 10-m height (a and b) 100-m height (c and d). For reference a r^{-1} decay (dotted) is shown on each plot.

Acknowledgments

REFERENCES

[1] Liu, W.T., K.B. Katsaros, and J.A. Businger, Bulk parameterization of air-sea exchanges of heat and water vapor including molecular constraints on the interface, *J. Atmospheric Sci.,* 36, pp. 1722–1735, 1979.

[2] Sylvester, J.J., G.C. Konstanzer, J.R. Rottier, G.D. Dockery, and J.R. Rowland, Aegis anti-air warfare tactical decision aids, *Johns Hopkins APL Tech. Digest,* 22(4), Oct.–Dec., 2001

[3] P. Gerstoft, L.T. Rogers, J. Krolik and W.S. Hodgkiss "Inversion for refractivity parameters from radar sea clutter", Radio Science, Vol 38, paper 18, pp 1-22, March 2003.

[4] P. Gerstoft, L.T. Rogers, W.S. Hodgkiss, and L.J Wagner "Refractivity estimation using multiple elevation angles" IEEE Oceanic Eng., July 2003.

[5] Barrios, A.E., "A terrain parabolic equation model for propagation in the troposphere," IEEE Trans. Antennas and Prop., 42(1),90–98, 1994

[6] Tarantola, A., *Inverse Problem Theory: Methods for Data Fitting and Parameter Estimation,* Elsevier, New York, 1987

[7] M.K. Sen and P.L. Stoffa, "Bayesian inference, Gibbs' sampler and uncertainty estimation in geophysical inversion," Geophys. Prospect. **44**, 313–350 (1996).

[8] P. Gerstoft and C.F. Mecklenbräuker, "Ocean acoustic inversion with estimation of *a posteriori* probability distributions," J. Acoust. Soc. Am. **104**(2):808–817, Aug. 1998.

[9] S.E Dosso, "Quantifying uncertainties in geoacoustic inversion. I a fast Gibbs sampler approach," J. Acoust. Soc. Am. **111**(1), 129–142 (2002).

[10] Mosegaard, K., and A. Tarantola, "Probabilistic approach to inverse problems," Chapter in *International Handbook of Earthquake and Engineering Seismology*, (http://web.ccr.jussieu.fr/tarantola/) (2002)

[11] Mosegaard K, Sambridge M., "Monte Carlo analysis of inverse problems." Inverse Problems **18**, no.3, , pp. 29–54 (2002)

[12] G.C. Konstanzer, "Large-scale Atmospheric Refractivity Range Interpolator (LARRI)," , 4–7 January 1999, URSI National Radio Science Meeting, Boulder, CO, 1999.